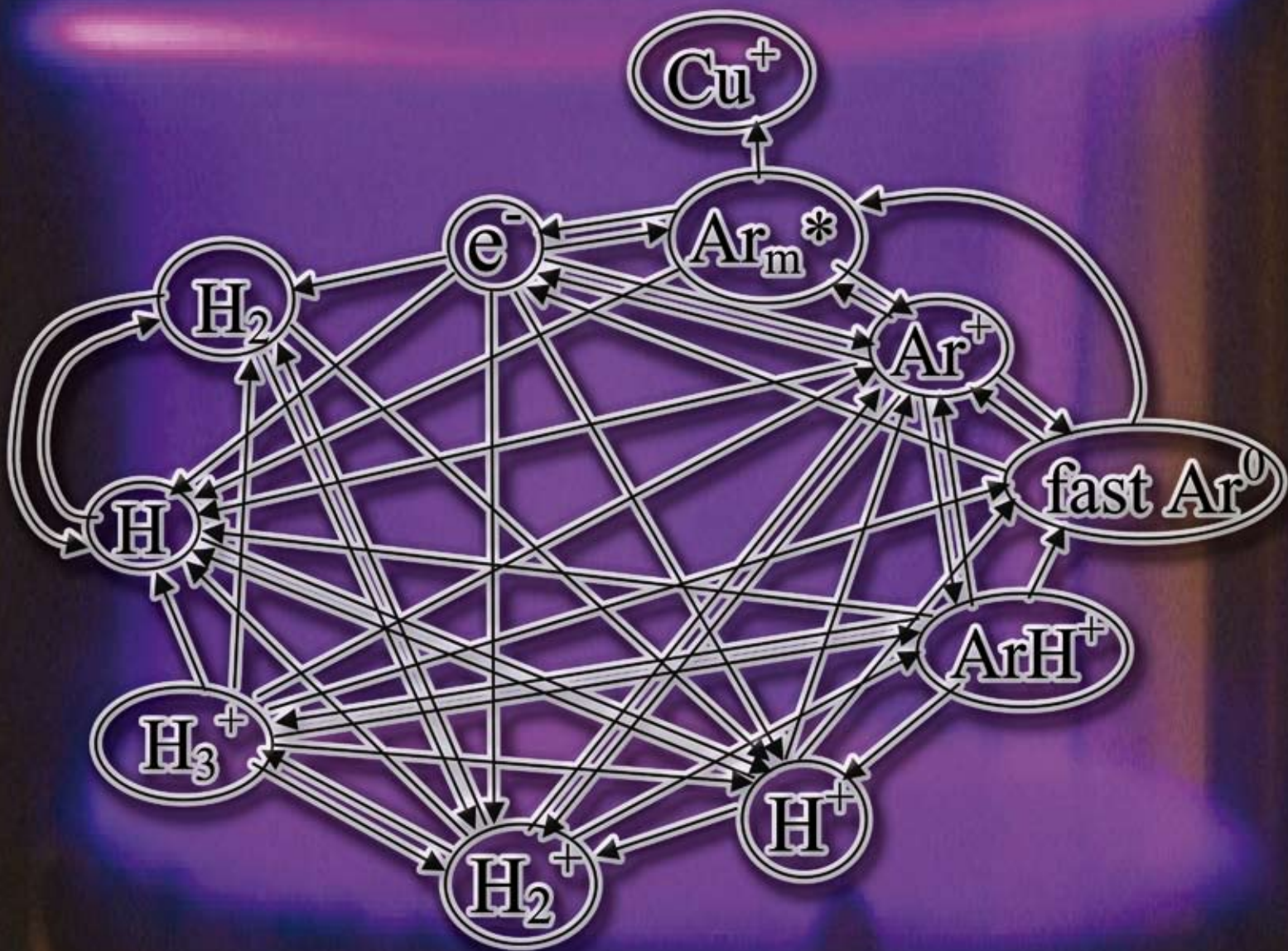


# JAAAS

Journal of Analytical Atomic Spectrometry

www.rsc.org/jaas

Volume 23 | Number 11 | November 2008 | Pages 1441–1556



ISSN 0267-9477

RSC Publishing

Bogaerts  
Computer simulations of  
argon-hydrogen Grimm-type  
glow discharges

Jakubowski *et al.*  
Labelling of proteins and antibodies  
and detection by LA-ICP-MS  
after gel electrophoresis and  
electroblotting—Parts I and II

# Computer simulations of argon–hydrogen Grimm-type glow discharges

Annemie Bogaerts\*

Received 23rd June 2008, Accepted 12th August 2008

First published as an Advance Article on the web 12th September 2008

DOI: 10.1039/b810599e

Computer simulations have been performed to describe the effect of small admixtures of hydrogen to an argon glow discharge in the Grimm-type configuration. The two-dimensional density profiles of the various plasma species (*i.e.*, electrons, Ar<sup>+</sup>, ArH<sup>+</sup>, H<sup>+</sup>, H<sub>2</sub><sup>+</sup> and H<sub>3</sub><sup>+</sup> ions, H atoms and H<sub>2</sub> molecules, Ar metastable atoms and sputtered Cu atoms) are presented for 1% H<sub>2</sub> added to the argon glow discharge, and the effect of different H<sub>2</sub> additions (varying between 0.1 and 10%) on the species densities, the hydrogen dissociation degree, and the sputtering process, are investigated. Finally, the relative contributions of various production and loss processes for the different plasma species are calculated.

## 1. Introduction

In the last decade, there has been increasing interest in the effects of small admixtures of hydrogen to argon glow discharges used for mass spectrometry and optical emission spectrometry.<sup>1–19</sup> Hydrogen Balmer lines have been investigated in Ar–H<sub>2</sub> mixtures in a Grimm-type glow discharge by Konjevic and coworkers<sup>1–3</sup> to obtain information on reactions in the plasma,<sup>1</sup> on the electron density<sup>2</sup> and on the electric field distribution.<sup>3</sup> Mason *et al.*<sup>4,5</sup> have studied the effect of H<sub>2</sub> on the ion intensities in a fast flowing glow discharge, with gas mixing close to the ion exit in order not to disturb the discharge. Furthermore, it appears that the relative sensitivity factors (RSFs) of different elements in glow discharge mass spectrometry (GDMS) are influenced by the addition of H<sub>2</sub>.<sup>6,7</sup> Indeed, a better correlation could be obtained between measured RSFs and values predicted by a simple empirical equilibrium model.<sup>6,7</sup> The Oviedo group has also published several papers on the effects of H<sub>2</sub> on the ion signals in GDMS, the sputtering rates and crater shapes<sup>8–11</sup> and on optical emission intensities in glow discharge optical emission spectrometry (GD-OES).<sup>12,13</sup> Hodoroaba *et al.* have thoroughly investigated the H<sub>2</sub> effect on optical emission intensities, and they observed that some optical emission line intensities increase while others decrease upon H<sub>2</sub> addition.<sup>14–16</sup> Weiss<sup>17</sup> reported that all Zn line intensities increase upon H<sub>2</sub> addition, but the effect is more significant for some lines than for others. This has important implications for the analysis of samples, where hydrogen is a major component of the sample, such as polymer coatings. Moreover, there are always some traces of hydrogen present in the glow discharge, arising from residual moisture in the source and on the sample surface, gaseous hydrocarbons coming from oil-pumps, leakage of water vapor through porous samples, *etc.* Therefore, it is clear that a thorough understanding of the role of hydrogen in argon glow discharges is highly important, so that corrections of the hydrogen effect can be accounted for in quantification algorithms, especially for the analysis of complex samples and thin films containing hydrogen. In ref. 18, Hodoroaba *et al.* have shown how the effect of H<sub>2</sub> can be exploited in

order to obtain better analytical figures of merit in GD-OES. Improvements in detection limits and in depth resolution for selected cases were reported. Recently, Steers *et al.*<sup>19</sup> have demonstrated that asymmetric charge transfer involving hydrogen ions is a very important selective excitation mechanism for spectral lines with a total excitation energy close to 13.6 eV. The magnitude of the effect varies for different elements and spectral lines. It is clear that great care should be taken before choosing ionic lines with a total excitation energy between 12.5–14 eV for analytical use.<sup>19</sup>

In previous work,<sup>20</sup> we have developed a comprehensive modeling network, describing the behavior of argon–hydrogen glow discharges. Up to now, the model was applied to the so-called VG9000 glow discharge source,<sup>20,21</sup> or to a simple cylindrical cell,<sup>22</sup> operating at relatively low gas pressure (75 and 133 Pa, respectively) and discharge current (1–2 and 5 mA, respectively). However, for applications of GD-OES, a Grimm-type source is most often used, which operates at much higher pressure and current (typically 400–1200 Pa and 10–50 mA). Therefore, our calculation results obtained for these low pressures and currents<sup>20–22</sup> are not necessarily valid for the typical conditions of GD-OES. For this reason, we have now applied our model to typical Grimm-type conditions, in order to investigate the effect of small admixtures of hydrogen on the argon discharge behavior, under conditions typically applied for GD-OES.

## 2. Description of the model

As the modeling network was developed earlier, and explained in detail in previous papers,<sup>20–22</sup> we will present here only a brief overview of the different plasma species included in the model, and the various chemical reactions they undergo. Table 1 summarizes the species taken into account in the modeling network, as well as the different submodels used to describe their behavior. The electrons are split up in a fast and a slow group, and the subdivision is defined based on the threshold for inelastic collisions. The fast electron trajectories and collisions are treated in a Monte Carlo model. The behavior of the slow electrons is described in a fluid model (*i.e.*, by solving a continuity equation based on different production and loss terms, as well as a transport equation based on diffusion and migration). This fluid

University of Antwerp, Department of Chemistry, Research group PLASMANT, Universiteitsplein 1, B-2610 Wilrijk-Antwerp, Belgium. E-mail: Annemie.Bogaerts@ua.ac.be

**Table 1** Overview of the species taken into account in the modeling network, and the models used to describe their behavior

| Plasma species                                      | Model                                       |
|---|---|
| Argon gas atoms                                     | no model                                    |
| Fast electrons                                      | Monte Carlo model                           |
| Slow electrons                                      | Fluid model                                 |
| Ar <sup>+</sup> ions                                | Fluid model                                 |
| ArH <sup>+</sup> ions                               | Monte Carlo model in the CDS<br>Fluid model |
| H <sup>+</sup> ions                                 | Monte Carlo model in the CDS<br>Fluid model |
| H <sub>2</sub> <sup>+</sup> ions                    | Monte Carlo model in the CDS<br>Fluid model |
| H <sub>3</sub> <sup>+</sup> ions                    | Monte Carlo model in the CDS<br>Fluid model |
| Fast Ar <sup>0</sup> atoms                          | Monte Carlo model in the CDS                |
| H atoms   | Fluid model                                 |
| H <sub>2</sub> molecules                            | Fluid model                                 |
| Ar metastable atoms (Ar <sub>m</sub> <sup>*</sup> ) | Fluid model                                 |
| Cu <sup>0</sup> sputtering                          | Empirical formula                           |
| Cu <sup>0</sup> atoms: thermalization               | Monte Carlo model                           |
| Thermal Cu <sup>0</sup> atoms                       | Fluid model                                 |

model treats also the various ions (Ar<sup>+</sup>, ArH<sup>+</sup>, H<sup>+</sup>, H<sub>2</sub><sup>+</sup> and H<sub>3</sub><sup>+</sup>) with similar equations, and finally it includes the Poisson equation, to obtain a self-consistent electric field distribution. Moreover, the trajectories and collisions of the various ions are also calculated in Monte Carlo models, in the cathode dark space (CDS) region in front of the cathode. Indeed, in this region a strong electric field is present, which accelerates the ions towards the cathode. Likewise, a similar Monte Carlo model is applied for the fast Ar atoms in this region, as they contribute to sputtering and to ionization and excitation of the Ar gas atoms. The behavior of the H<sub>2</sub> molecules and H atoms is described again with a fluid model, containing continuity (or balance) equations with different production and loss terms and transport equations based on diffusion. A similar fluid model is also applied to the Ar metastable atoms (denoted here as Ar<sub>m</sub><sup>\*</sup>) and the sputtered (thermal) Cu atoms. Before applying this fluid model, the sputtered Cu atoms first need to become thermalized, a situation which is treated with a Monte Carlo model. The sputtering flux itself is obtained based on the calculated flux energy distributions of the various ions and the fast Ar atoms bombarding the cathode, in combination with an empirical formula for the sputtering yield as a function of bombarding energy.<sup>23</sup> All these models are coupled to each other and solved iteratively until convergence is reached, as explained in detail in ref. 20, to obtain an overall picture of the glow discharge plasma.

The collisions and chemical reactions of the various species taken into account in this model are listed in Table 2. Note that the collision rates, as calculated in the various Monte Carlo models, serve also as production and loss terms in the fluid models. Again, full details of all these reactions, their cross sections or rate coefficients, and the references where the data were taken from, can be found in ref 20. Here we should point out only one difference with respect to our previous model, *i.e.*, for the rate coefficient of ArH<sup>+</sup>-electron dissociative recombination. In our previous model, we assumed a value of  $k = 10^{-7} \text{ cm}^3 \text{ s}^{-1}$ , based on ref. 24. Indeed, this value is typical for dissociative recombination of many diatomic molecular ions.

However, it was pointed out in a more recent paper<sup>25</sup> that ArH<sup>+</sup> is one of the rare molecular ions that does not exhibit a higher recombination rate at low electron energies. A rate coefficient was measured by means of storage ring experiments in the order of  $10^{-10} \text{ cm}^3 \text{ s}^{-1}$  at low electron energies, and varying between  $10^{-9}$  and  $10^{-8} \text{ cm}^3 \text{ s}^{-1}$  for energies between 2.5 and 35 eV.<sup>25</sup> Hence, instead of the earlier value of  $k = 10^{-7} \text{ cm}^3 \text{ s}^{-1}$  as applied in our previous model, we assume now a value of  $k = 5 \times 10^{-10} \text{ cm}^3 \text{ s}^{-1}$  for electron-ion dissociative recombination of ArH<sup>+</sup> ions. A more accurate, *e.g.* energy-dependent, value for this rate coefficient is not necessary, as this process turns out not to be of major importance in the discharge (see section 3.2 below).

Besides the collisions in the plasma, also processes occurring at the cathode and the anode cell walls are taken into account in the calculations, such as sputtering (see above), secondary electron emission, and sticking or reflection of the various plasma species. For the ions, it is assumed that they become neutralized at the cell walls (after having given rise to secondary electron emission and sputtering) and either adsorb or return to the plasma as neutrals. The Ar<sub>m</sub><sup>\*</sup> metastable atoms are assumed to become de-excited at the walls. The electrons can become absorbed, cause secondary electron emission or become (elastically or inelastically) reflected. The sputtered Cu atoms are assumed to be deposited or reflected at the anode and cathode, based on a sticking coefficient of 0.5. Finally, for the H atoms, a fraction of them will recombine at the walls into H<sub>2</sub> molecules. This recombination coefficient is found to be in the order of 0.1–0.25 for most metal surfaces.<sup>26</sup> We assumed a recombination coefficient of 0.1, as in our previous calculations (see ref. 20 for more explanations).

Calculations are performed for typical operating conditions of a Grimm-type glow discharge, *i.e.*, 800 V discharge voltage, about 30 mA electrical current, and 850 Pa argon gas pressure, with H<sub>2</sub> admixtures ranging from 0.1 till 10%. Note that the argon gas is considered stationary at a constant temperature. Hence, no gas heating or gas flow is taken into account in these calculations. Indeed, this makes the model setup much more complicated, and it is not so essential to understand the plasma chemistry in the Ar–H<sub>2</sub> gas mixture.

### 3. Results and discussion

#### 3.1. Number densities of the plasma species

Fig. 1 presents the two-dimensional (2D) number density profiles of the electrons and the various ions, in the case of 1% H<sub>2</sub> added to the Ar gas. Note that the cathode is found at the left border of the figures, whereas the upper and lower figure borders represent the anode (source) walls. The discharge extends after 1 cm length, but as most densities become negligible for longer distances from the cathode, we show only the first cm. It is clear that the densities of electrons and ions reach a maximum around 0.5 mm from the cathode, which corresponds to the beginning of the negative glow (NG) region. The electron density is virtually zero in the CDS, whereas the ions reach low but constant values in this region, resulting in a positive space charge, which gives rise to the strong electric field that is so characteristic for the CDS. In the remaining part of the discharge, the electron density is equal to the sum of the positive ion densities, to ensure charge neutrality. The Ar<sup>+</sup> ions exhibit clearly the highest density of all

**Table 2** Reactions taken into account in the model, for the various plasma species<sup>a</sup>

|                                  |  |   |
|----------------------------------|--|---|
| Electron reactions               |  |   |
| 1                                | $e^- + \text{Ar} \rightarrow e^- + \text{Ar}$  | Elastic scattering  |
| 2                                | $e^- + \text{Ar} \rightarrow e^- + \text{Ar}^+ + e^-$  | Ionization  |
| 3                                | $e^- + \text{Ar} \rightarrow e^- + \text{Ar}^* (\text{incl. Ar}_m^*)$                              | Total excitation (incl. to the $\text{Ar}_m^*$ levels)                |
| 4                                | $e^- + \text{Ar}_m^* \rightarrow e^- + \text{Ar}^+ + e^-$  | Ionization from the $\text{Ar}_m^*$ levels                            |
| 5                                | $e^- + \text{Ar}_m^* \rightarrow e^- + \text{Ar}^*$  | Total excitation from the $\text{Ar}_m^*$ levels                      |
| 6                                | $e^- + \text{Ar}_m^* \rightarrow e^- + \text{Ar}_r^*$  | Electron quenching of the $\text{Ar}_m^*$ levels                      |
| 7                                | $e^- + \text{H}_2 \rightarrow e^- + \text{H}_2$  | Elastic scattering  |
| 8                                | $e^- + \text{H}_2 \rightarrow e^- + \text{H}_2^* (\text{v})$                                       | Total vibrational excitation  |
| 9                                | $e^- + \text{H}_2 \rightarrow e^- + \text{H}_2^* (\text{s})$                                       | Total electron excitation to singlet states                           |
| 10                               | $e^- + \text{H}_2 \rightarrow e^- + \text{H}_2^* (\text{t}) \rightarrow e^- + \text{H} + \text{H}$ | Total electron excitation to triplet states, followed by dissociation |
| 11                               | $e^- + \text{H}_2 \rightarrow e^- + \text{H}_2^+ + e^-$  | Ionization  |
| 12                               | $e^- + \text{H}_2 \rightarrow e^- + \text{H}^+ + \text{H} + e^-$                                   | Dissociative ionization   |
| 13                               | $e^- + \text{H} \rightarrow e^- + \text{H}^*$  | Total excitation  |
| 14                               | $e^- + \text{H} \rightarrow e^- + \text{H}^+ + e^-$  | Ionization  |
| 15                               | $e^- + \text{Cu} \rightarrow e^- + \text{Cu}^+ + e^-$  | Ionization  |
| 16                               | $e^- + \text{ArH}^+ \rightarrow \text{Ar} + \text{H}$  | Recombination   |
| 17                               | $e^- + \text{H}_2^+ \rightarrow \text{H} + \text{H}$   | Recombination   |
| 18                               | $e^- + \text{H}_3^+ \rightarrow \text{H} + \text{H} + \text{H} \text{ or } \text{H}_2 + \text{H}$  | Recombination   |
| Reactions of $\text{Ar}^+$ ions  |  |   |
| 19                               | $\text{Ar}^+ + \text{Ar} \rightarrow \text{Ar}^+ + \text{fast Ar}$                                 | Elastic scattering, incl. symmetric charge transfer                   |
| 20                               | $\text{Ar}^+ + \text{Ar} \rightarrow \text{Ar}^+ + \text{Ar}^+ + e^-$                              | Ionization  |
| 21                               | $\text{Ar}^+ + \text{Ar} \rightarrow \text{Ar}^+ + \text{Ar}_m^*$                                  | Excitation to the $\text{Ar}_m^*$ levels                              |
| 22                               | $\text{Ar}^+ + \text{H}_2 \rightarrow \text{ArH}^+ + \text{H}$                                     | H-atom transfer   |
| 23                               | $\text{Ar}^+ + \text{H}_2 \rightarrow \text{fast Ar} + \text{H}_2^+$                               | Asymmetric charge transfer  |
| Reactions of $\text{ArH}^+$ ions |  |   |
| 24                               | $\text{ArH}^+ + \text{Ar} \rightarrow \text{ArH}^+ + \text{fast Ar}$                               | Elastic scattering  |
| 25                               | $\text{ArH}^+ + \text{Ar} \rightarrow \text{fast Ar} + \text{H}^+ + \text{Ar}$                     | Collision-induced dissociation  |
| 26                               | $\text{ArH}^+ + \text{Ar} \rightarrow \text{fast Ar}^+ + \text{H} + \text{Ar}$                     | Collision-induced dissociation  |
| 27                               | $\text{ArH}^+ + \text{H}_2 \rightarrow \text{ArH}^+ + \text{fast H}_2$                             | Elastic scattering  |
| 28                               | $\text{ArH}^+ + \text{H}_2 \rightarrow \text{fast Ar} + \text{H}_3^+$                              | Proton transfer   |
| 29                               | $\text{ArH}^+ (\text{at walls}) \rightarrow 0.6 \text{ H}$   | Reflection (+ neutralization/dissociation)                            |
| 16                               | $e^- + \text{ArH}^+ \rightarrow \text{Ar} + \text{H}$  | Recombination   |
| Reactions of $\text{H}^+$ ions   |  |   |
| 30                               | $\text{H}^+ + \text{Ar} \rightarrow \text{H}^+ + \text{fast Ar}$                                   | Elastic scattering  |
| 31                               | $\text{H}^+ + \text{Ar} \rightarrow \text{fast H} + \text{Ar}^+$                                   | Asymmetric charge transfer  |
| 32                               | $\text{H}^+ + \text{H} \rightarrow \text{fast H} + \text{H}^*$                                     | Symmetric charge transfer   |
| 33                               | $\text{H}^+ + \text{H}_2 \rightarrow \text{H}^+ + \text{H}_2^*$                                    | Total vibrational excitation  |
| 34                               | $\text{H}^+ + \text{H}_2 \rightarrow \text{H}^+ + \text{fast H}_2$                                 | Elastic scattering  |
| 35                               | $\text{H}^+ + \text{H}_2 \rightarrow \text{fast H} + \text{H}_2^+$                                 | Asymmetric charge transfer  |
| 36                               | $\text{H}^+ (\text{at walls}) \rightarrow 0.6 \text{ H}$   | Reflection (+ neutralization)   |
| Reactions of $\text{H}_2^+$ ions |  |   |
| 37                               | $\text{H}_2^+ + \text{Ar} \rightarrow \text{H} + \text{ArH}^+$                                     | Proton transfer   |
| 38                               | $\text{H}_2^+ + \text{Ar} \rightarrow \text{fast H}_2 + \text{Ar}^+$                               | Asymmetric charge transfer  |
| 39                               | $\text{H}_2^+ + \text{H}_2 \rightarrow \text{H} + \text{H}_3^+$                                    | Proton transfer   |
| 40                               | $\text{H}_2^+ + \text{H}_2 \rightarrow \text{fast H}_2 + \text{H}_2^+$                             | Symmetric charge transfer   |
| 41                               | $\text{H}_2^+ (\text{at walls}) \rightarrow 1.2 \text{ H}$   | Reflection (+ neutralization/dissociation)                            |
| 17                               | $e^- + \text{H}_2^+ \rightarrow \text{H} + \text{H}$   | Recombination   |
| Reactions of $\text{H}_3^+$ ions |  |   |
| 42                               | $\text{H}_3^+ + \text{Ar} \rightarrow \text{H}_3^+ + \text{fast Ar}$                               | Elastic scattering  |
| 43                               | $\text{H}_3^+ + \text{Ar} \rightarrow \text{fast H}_2 + \text{slow ArH}^+$                         | Proton transfer   |
| 44                               | $\text{H}_3^+ + \text{Ar} \rightarrow \text{fast H}_2 + \text{fast H} + \text{slow Ar}^+$          | Charge transfer + dissociation  |
| 45                               | $\text{H}_3^+ + \text{Ar} \rightarrow \text{fast H}^+ + \text{fast H}_2 + \text{slow Ar}$          | Collision-induced dissociation  |
| 46                               | $\text{H}_3^+ + \text{Ar} \rightarrow \text{fast H}_2^+ + \text{fast H} + \text{slow Ar}$          | Collision-induced dissociation  |
| 47                               | $\text{H}_3^+ + \text{H}_2 \rightarrow \text{H}_3^+ + \text{fast H}_2$                             | Elastic scattering  |
| 48                               | $\text{H}_3^+ + \text{H}_2 \rightarrow \text{fast H}_2 + \text{slow H}_3^+$                        | Proton transfer   |
| 49                               | $\text{H}_3^+ + \text{H}_2 \rightarrow \text{fast H}_2 + \text{slow H}_2 + \text{slow H}^+$        | Proton transfer + dissociation  |
| 50                               | $\text{H}_3^+ + \text{H}_2 \rightarrow \text{fast H}_2 + \text{slow H} + \text{slow H}_2^+$        | Proton transfer + dissociation  |
| 51                               | $\text{H}_3^+ + \text{H}_2 \rightarrow \text{fast H}_2 + \text{fast H} + \text{slow H}_2^+$        | Charge transfer + dissociation  |
| 52                               | $\text{H}_3^+ + \text{H}_2 \rightarrow \text{fast H}_2^+ + \text{fast H} + \text{slow H}_2$        | Collision-induced dissociation  |
| 53                               | $\text{H}_3^+ + \text{H}_2 \rightarrow \text{fast H}^+ + \text{fast H}_2 + \text{slow H}_2$        | Collision-induced dissociation  |
| 54                               | $\text{H}_3^+ + \text{H}_2 \rightarrow \text{fast H}^+ + 2 \text{ fast H} + \text{slow H}_2$       | Collision-induced dissociation  |
| 55                               | $\text{H}_3^+ (\text{at walls}) \rightarrow 1.8 \text{ H}$   | Reflection (+ neutralization/dissociation)                            |
| 18                               | $e^- + \text{H}_3^+ \rightarrow \text{H} + \text{H} + \text{H} \text{ or } \text{H}_2 + \text{H}$  | Recombination   |
| Reactions of fast Ar atoms       |  |   |
| 56                               | $\text{fast Ar} + \text{slow Ar} \rightarrow \text{fast Ar} + \text{fast Ar}$                      | Elastic scattering  |
| 57                               | $\text{fast Ar} + \text{slow Ar} \rightarrow \text{fast Ar} + \text{Ar}^+ + e^-$                   | Ionization  |
| 58                               | $\text{fast Ar} + \text{slow Ar} \rightarrow \text{fast Ar} + \text{Ar}_m^*$                       | Excitation to the $\text{Ar}_m^*$ levels                              |

**Table 2** (Contd.)

Reactions of Ar<sub>m</sub><sup>\*</sup> metastable atoms

|    |  |   |
|----|--|---|
| 4  | Ar <sub>m</sub> <sup>*</sup> + e <sup>-</sup> → Ar <sup>+</sup> + 2 e <sup>-</sup>                               | Electron impact ionization  |
| 5  | Ar <sub>m</sub> <sup>*</sup> + e <sup>-</sup> → Ar <sup>*</sup> + e <sup>-</sup>                                 | Electron impact excitation  |
| 6  | Ar <sub>m</sub> <sup>*</sup> + e <sup>-</sup> → Ar <sub>r</sub> <sup>*</sup> + e <sup>-</sup>                    | Electron quenching (transfer to a nearby radiative level, which will decay to the ground state) |
| 59 | Ar <sub>m</sub> <sup>*</sup> + Ar <sub>m</sub> <sup>*</sup> → Ar <sup>0</sup> + Ar <sup>+</sup> + e <sup>-</sup> | Metastable-metastable collision   |
| 60 | Ar <sub>m</sub> <sup>*</sup> + Cu <sup>0</sup> → Ar <sup>0</sup> + Cu <sup>+</sup> + e <sup>-</sup>              | Penning ionization of Cu  |
| 61 | Ar <sub>m</sub> <sup>*</sup> + Ar <sup>0</sup> → Ar <sup>0</sup> + Ar <sup>0</sup>                               | Two-body collision  |
| 62 | Ar <sub>m</sub> <sup>*</sup> + 2 Ar <sup>0</sup> → Ar <sub>2</sub> <sup>*</sup> + Ar <sup>0</sup>                | Three-body collision  |
| 63 | Ar <sub>m</sub> <sup>*</sup> + H <sub>2</sub> → Ar + H + H   | Quenching by dissociation of H <sub>2</sub>   |
| 64 | Ar <sub>m</sub> <sup>*</sup> + H → Ar + H <sup>*</sup>   | Excitation of H   |
| 65 | Ar <sub>m</sub> <sup>*</sup> (at walls) → Ar   | De-excitation at walls  |

<sup>a</sup> Note that reactions 4–6 and reactions 16–18 occur twice in the table, because they apply to two types of reactive species, *i.e.*, electrons and Ar<sub>m</sub><sup>\*</sup> metastables, or electrons and ions. The reactions involving H<sub>2</sub> molecules, H atoms and sputtered Cu atoms are not separately listed anymore, as they occur always with another reactive species, and are hence already included in the table. The only exception is: (66) recombination at the walls (H + H(walls) → H<sub>2</sub>), with an assumed recombination factor of  $\gamma = 0.1$ .

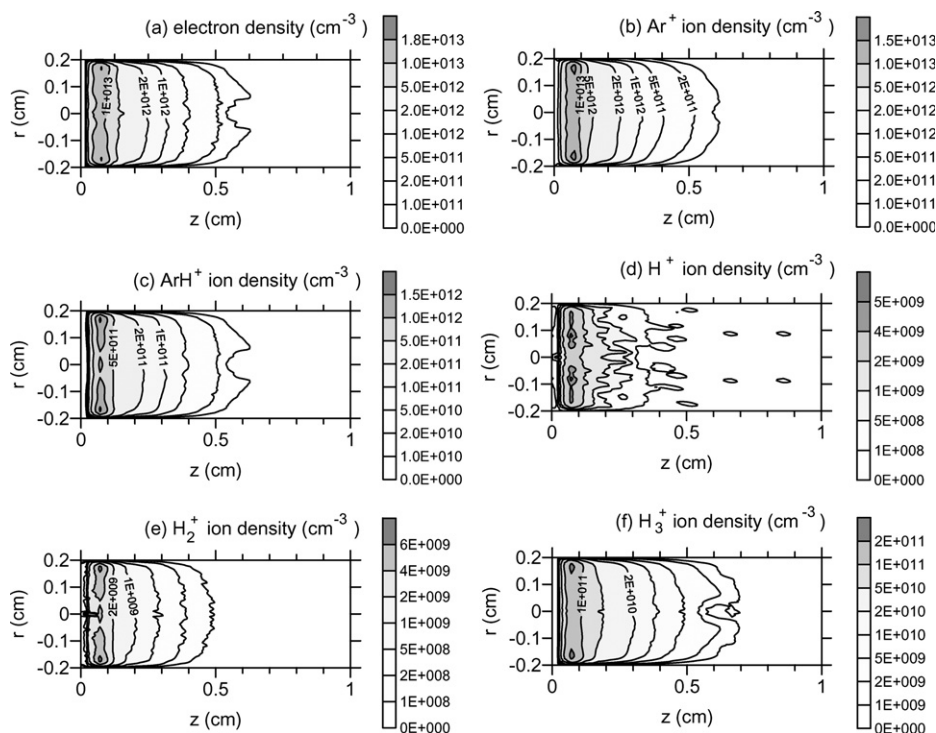


**Fig. 1** Calculated two-dimensional density profiles of the electrons (a), Ar<sup>+</sup> (b), ArH<sup>+</sup> (c), H<sup>+</sup> (d), H<sub>2</sub><sup>+</sup> (e) and H<sub>3</sub><sup>+</sup> (f) ions, in a Grimm-type source, operating at 800 V, 30 mA, 850 Pa Ar pressure with 1% H<sub>2</sub> addition.

positive ions. The densities of the ArH<sup>+</sup> and H<sub>3</sub><sup>+</sup> ions are about one and two orders of magnitude lower, respectively, whereas the H<sup>+</sup> and H<sub>2</sub><sup>+</sup> ions have still lower densities, and can be considered negligible.

These results are, at least qualitatively, consistent with findings in the literature. Indeed, it is reported for pure hydrogen discharges<sup>26,27</sup> that H<sup>+</sup> and H<sub>2</sub><sup>+</sup> ions react rapidly in low-field regions with H<sub>2</sub> molecules to form H<sub>3</sub><sup>+</sup> ions, which do not fragment again, until they move into higher field regions. H<sub>3</sub><sup>+</sup> ions are therefore the dominant hydrogen ions in low-field hydrogen plasmas.<sup>27,28</sup> This was also reported in GDMS, where a strong peak was observed in the mass spectrum at  $m/z = 3$ ,

corresponding to H<sub>3</sub><sup>+</sup> ions.<sup>8</sup> Likewise, the ArH<sup>+</sup> ion intensities in the mass spectrum can sometimes be found of the same magnitude or even higher than the Ar<sup>+</sup> ion intensity, when small amounts of H<sub>2</sub> (or H<sub>2</sub>O) are added to the argon glow discharge.<sup>6,29</sup>

The effect of different H<sub>2</sub> additions on the electron and various ion number densities (at the maximum of their profiles) is illustrated in Fig. 2. The Ar<sup>+</sup> ion density decreases upon H<sub>2</sub> addition, whereas the other ion densities increase, as expected. Indeed, the Ar<sup>+</sup> ions are transferred into the other (hydrogen-related) ions, mainly by H-atom transfer (reaction (22) of Table 2). This gives rise to the formation of ArH<sup>+</sup> ions, which on their turn give rise

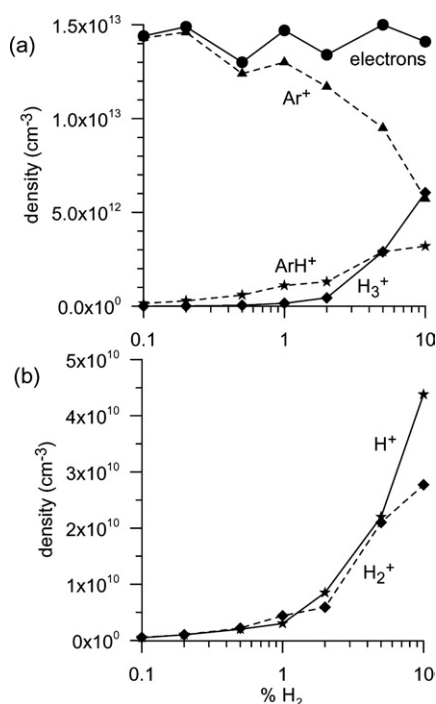


**Fig. 2** Densities of electrons and the various ions, calculated at the maximum of their profiles, as a function of H<sub>2</sub> addition to the Ar gas, for the same conditions as in Fig. 1.

to H<sub>3</sub><sup>+</sup> ions by proton-transfer with H<sub>2</sub> (reaction (28) of Table 2). The H<sup>+</sup> and H<sub>2</sub><sup>+</sup> ions are also created from ArH<sup>+</sup>, H<sub>3</sub><sup>+</sup> and Ar<sup>+</sup> ions, but to a lower extent (see further details below in section 3.2). It should be noticed that in our previous simulations, the ArH<sup>+</sup>, H<sup>+</sup>, H<sub>2</sub><sup>+</sup> and H<sub>3</sub><sup>+</sup> ions exhibited a maximum density at a certain H<sub>2</sub> concentration, whereafter the densities dropped again, because of increasing importance of certain loss mechanisms compared to production mechanisms.<sup>21</sup> The fact that our current simulations for the Grimm-type source do not predict this behavior, illustrates that the hydrogen effect is clearly

dependent on the discharge conditions (mainly the source pressure). It is also worthwhile to notice that the calculations do not predict a strong drop in the Ar<sup>+</sup> ion density between 0.1 and 1% H<sub>2</sub> addition. This is somewhat in contrast to the experimental data, where excitation of some species is strongly affected at hydrogen concentrations as low as 0.3%. For example, Hodoroaba *et al.* have observed that the Cu II line at 224.7 nm, which is excited by charge transfer with Ar<sup>+</sup> metastable ions, drops in intensity by a factor of *ca.* 5 in Ar–0.3% H<sub>2</sub>, relatively to a pure Ar discharge.<sup>14</sup>

Because of the decreasing trend of Ar<sup>+</sup> ion densities and the corresponding rise in the other ion densities, the electron density remains more or less constant, as appears from Fig. 2(a). Consequently, the electrical current, which is carried by the electrons and all positive ions, was also calculated to remain more or less constant around 30 mA. This result is clearly different from our previous results,<sup>21</sup> where a drop in electron densities and electrical current was predicted. The reason is probably due to the lower rate coefficient for ArH<sup>+</sup>–electron dissociative recombination, compared to our previous model (see section 2 above). Indeed, previously, Ar<sup>+</sup> ions were transferred into ArH<sup>+</sup> ions, which could then be neutralized by recombination with electrons, resulting in a lower degree of ionization at higher H<sub>2</sub> concentrations. In the present model, this recombination becomes almost negligible, so that the electron density and the electrical current remain more or less constant.

The 2D number density profiles of the neutral plasma species, *i.e.*, H<sub>2</sub> molecules, H atoms, Ar<sub>m</sub><sup>\*</sup> metastable atoms and sputtered Cu atoms, are presented in Fig. 3. The H<sub>2</sub> number density is in the order of 1.5–2 × 10<sup>15</sup> cm<sup>-3</sup>, which corresponds indeed to a fraction of 1% of the total Ar density, at a gas pressure of 850 Pa. However, the density is slightly depleted near the cathode, as a result of dissociation (mainly upon collisions with Ar<sub>m</sub><sup>\*</sup> atoms, see below in section 3.2). Consequently, the H atoms exhibit a maximum density at about 1 mm from the cathode. It should be noticed that the maximum H atom density is only about one order of magnitude lower than the H<sub>2</sub> density, but because it drops more

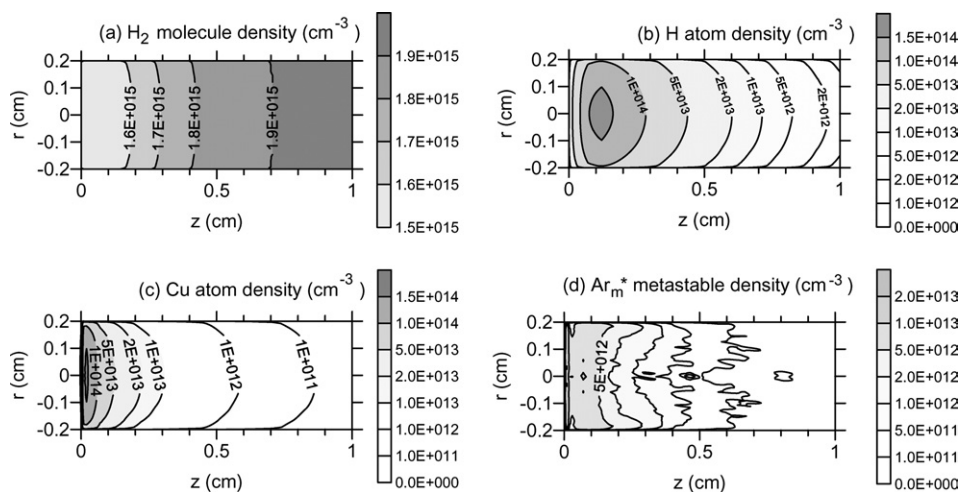


**Fig. 3** Calculated two-dimensional density profiles of the H<sub>2</sub> molecules (a), H atoms (b), sputtered Cu atoms (c) and Ar<sub>m</sub><sup>\*</sup> metastable atoms (d), for the same conditions as in Fig. 1.

rapidly as a function of distance from the cathode, the overall density is about two orders of magnitude lower, resulting in a dissociation degree calculated to be 1.5% at the present conditions. This value is significantly higher than the dissociation degree calculated for typical VG9000 GDMS conditions (*i.e.*, in the order of 0.01–0.05%).<sup>21</sup> The reason is that the Grimm source operates at much higher pressure (*i.e.*, 850 Pa in the present study, *versus* about 50–100 Pa for VG9000 conditions), which results in a drastic increase in the number of collisions, giving rise to dissociation of the H<sub>2</sub> gas.

For comparison, the sputtered Cu atom and Ar<sub>m</sub>\* metastable atom densities are also presented in Fig. 3. It appears that the H atoms are characterized by more or less the same density as the sputtered Cu atoms, at least at the maximum of their profiles. However, the Cu atom density drops more rapidly as a function of distance from the cathode in comparison to the H atom density. Hence, overall the H atom density in the discharge is higher than the sputtered Cu atom density. The Ar<sub>m</sub>\* atoms have a much lower density than the H atoms and sputtered Cu atoms. It is more comparable to the electron density, but it reaches a pronounced maximum only in front of the cathode, as a result of fast Ar<sup>+</sup> ion and Ar<sup>0</sup> atom impact excitation (see below in section 3.2).

In Fig. 4, the densities of H<sub>2</sub> molecules and H atoms, at the maximum of their profiles, are plotted as a function of the H<sub>2</sub> addition. It appears that both rise more or less to the same extent: the H<sub>2</sub> molecule density increases of course linearly with rising H<sub>2</sub> addition, whereas the H atom density rises only slightly less than linearly. Indeed, the dissociation degree of H<sub>2</sub> is calculated to be in the order of 1–2%, decreasing slightly with higher H<sub>2</sub> concentrations, as is depicted in Fig. 5. Note that the dissociation degree shown in Fig. 5 is not obtained simply by dividing the maximum H density by the maximum H<sub>2</sub> density, but rather by dividing the densities, integrated over the whole discharge region, as this gives a more realistic picture of the overall amount of dissociation. It should be noticed that this calculated dissociation degree of 1–2% is clearly different from our calculation results obtained previously for the VG9000 GDMS conditions, where the dissociation degree was much lower, *i.e.*, in the order of only 0.01–0.05%, and clearly decreasing with H<sub>2</sub> concentration. The reason was already pointed out above: the Grimm-type source

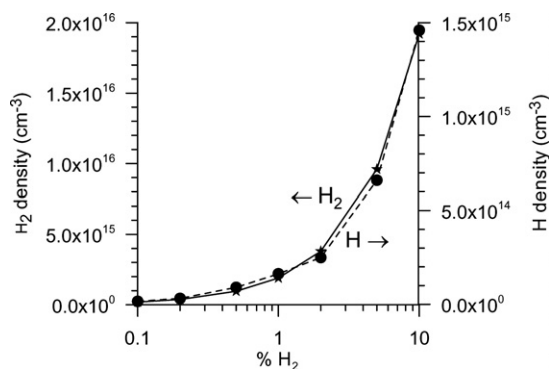


**Fig. 4** Densities of H<sub>2</sub> molecules (solid lines, \* symbols, left axis) and H atoms (dashed lines, • symbols, right axis), calculated at the maximum of their profiles, as a function of H<sub>2</sub> addition to the Ar gas, for the same conditions as in Fig. 1.

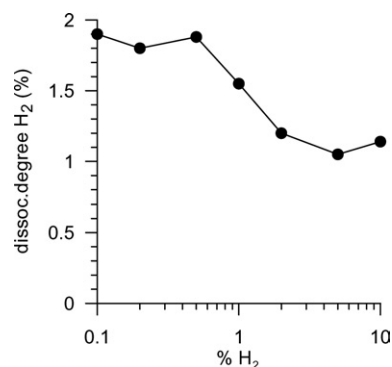


**Fig. 5** Calculated dissociation degree of H<sub>2</sub> molecules as a function of H<sub>2</sub> addition to the Ar gas, for the same conditions as in Fig. 1.

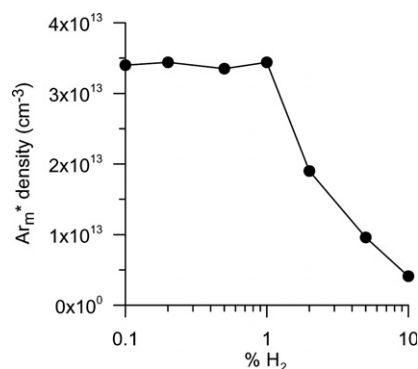
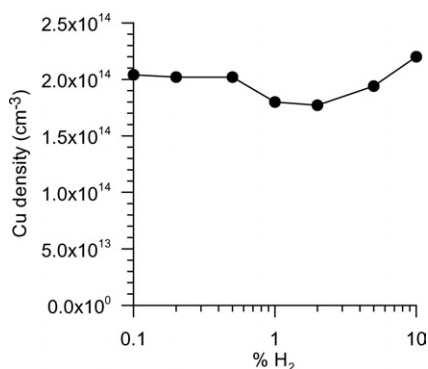


**Fig. 6** Ar<sub>m</sub>\* metastable density, calculated at the maximum of its profile, as a function of H<sub>2</sub> addition to the Ar gas, for the same conditions as in Fig. 1.

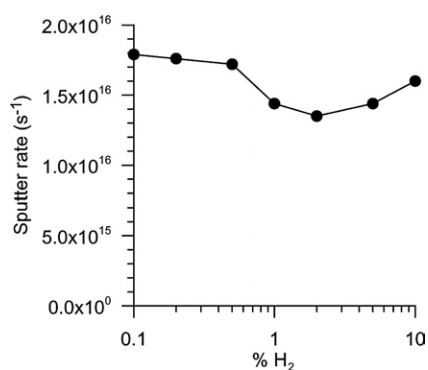
operates at much higher pressures, where collisions are more important, including dissociation of the H<sub>2</sub> molecules.

Fig. 6 illustrates that the calculated Ar<sub>m</sub>\* density is more or less constant until 1% H<sub>2</sub> addition, but then drops dramatically for higher H<sub>2</sub> concentrations. This is attributed to quenching of the Ar<sub>m</sub>\* metastable level upon collisions with H<sub>2</sub> molecules, a loss process which becomes predominant at H<sub>2</sub> concentrations above 1% (see below in section 3.2).

The sputtered Cu atom density, at the maximum of its profile, is plotted against H<sub>2</sub> concentration in Fig. 7. It is more or less constant, with a small dip around 1–2% H<sub>2</sub> addition. This is attributed to the sputtering rate, which exhibits the same behavior, as can be observed from Fig. 8. The reason for this behavior is as follows. The sputtering is caused by the fluxes of the various ions and the fast Ar atoms bombarding the cathode. The ion fluxes increase or decrease in the same way as the corresponding densities, *i.e.*, the Ar<sup>+</sup> ion flux decreases, whereas the fluxes of ArH<sup>+</sup>, H<sup>+</sup>, H<sub>2</sub><sup>+</sup> and H<sub>3</sub><sup>+</sup> ions increase upon H<sub>2</sub> addition. Consequently, at low H<sub>2</sub> concentrations, the Ar<sup>+</sup> ions, together with the fast Ar<sup>0</sup> atoms, are the dominant sputtering species, as is clear from Fig. 9. However, the role of ArH<sup>+</sup> ions rises for higher H<sub>2</sub> concentrations, whereas the contribution of Ar<sup>+</sup> ions decreases. These two opposite effects result in a nearly constant sputtering rate, with a small dip at H<sub>2</sub> concentrations of about 1–2%. Note that the H<sup>+</sup>, H<sub>2</sub><sup>+</sup> and H<sub>3</sub><sup>+</sup> ions play a negligible role in the sputtering process, due to the large mass difference.



**Fig. 7** Sputtered Cu atom density, calculated at the maximum of its profile, as a function of H<sub>2</sub> addition to the Ar gas, for the same conditions as in Fig. 1.



**Fig. 8** Calculated sputtering rate as a function of H<sub>2</sub> addition to the Ar gas, for the same conditions as in Fig. 1.

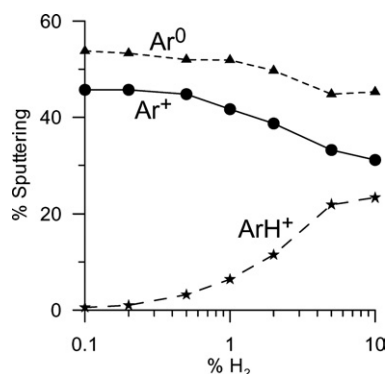


**Fig. 9** Calculated relative contributions of Ar<sup>+</sup> ions, fast Ar<sup>0</sup> atoms and ArH<sup>+</sup> ions to the sputtering process, as a function of H<sub>2</sub> addition to the Ar gas, for the same conditions as in Fig. 1.

Finally, the relative contributions of electron impact ionization (EI), Penning ionization (PI) and asymmetric charge transfer (CT) to the ionization of the sputtered Cu atoms are plotted in Fig. 10. It is found that PI is the dominant ionization mechanism for H<sub>2</sub> concentrations up till 1–2%. CT is found to be of secondary importance, closely followed by EI. However, for H<sub>2</sub> concentrations above 2%, the relative contribution of PI

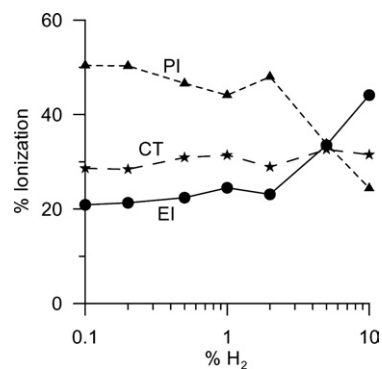


**Fig. 10** Calculated relative contributions of Penning ionization (PI), asymmetric charge transfer (CT) and electron impact ionization (EI) to the ionization of the sputtered Cu atoms, as a function of H<sub>2</sub> addition to the Ar gas, for the same conditions as in Fig. 1.

decreases, because of the significant drop in Ar<sub>m</sub><sup>\*</sup> metastable density (cf. Fig. 6 above). Electron impact ionization, on the other hand, rises above H<sub>2</sub> concentrations of 2%, and is even of major importance for the H<sub>2</sub> concentration of 10%, as appears from Fig. 10. Note, however, that these relative contributions are only approximate values, since the rate coefficients of Penning ionization and asymmetric charge transfer are subject to considerable uncertainties. Nevertheless, the trend of increasing relative importance of electron impact ionization is expected to be correctly predicted.

This result might explain the observations made in the literature<sup>6,7</sup> that in Ar–H<sub>2</sub> glow discharges a better correlation could be obtained between measured RSFs in GDMS and values predicted by simple empirical equilibrium models, based on the first ionization potential of the elements. The latter plays a role only in the cross section of electron impact ionization, but not in the rate coefficients for Penning ionization and asymmetric charge transfer. Hence, this better correlation with the simple model predictions suggests that electron impact ionization plays a more prominent role as an ionization mechanism of the sputtered atoms in the Ar–H<sub>2</sub> discharge compared to a pure Ar discharge, which is, at least qualitatively, in accordance with our model predictions.

### 3.2. Relative role of different production and loss processes for the plasma species

Table 3 gives an overview of the relative contributions of the most important production and loss processes for the various plasma species, calculated for 1% H<sub>2</sub> addition. The electrons are predominantly formed by electron impact ionization of Ar, as is also the case in pure Ar discharges, and they are lost mainly by recombination with H<sub>3</sub><sup>+</sup> ions. Indeed, recombination with H<sup>+</sup> and H<sub>2</sub><sup>+</sup> ions is of minor importance, because of the much lower densities of these ions, and recombination with ArH<sup>+</sup> ions is also less important because of the lower rate coefficient (see section 2 above). This result is different from our previous calculations<sup>20</sup> where the same rate coefficients for recombination with H<sub>3</sub><sup>+</sup> and ArH<sup>+</sup> ions were assumed, and where it was predicted that both processes contribute for about 60 and 40%, respectively. We have repeated our previous calculations for the VG9000 GDMS

**Table 3** Calculated relative contributions of the most important production and loss processes for the various plasma species. The numbers between brackets after each production or loss process correspond to the reactions listed in Table 2, to visualize the meaning of the processes

| Production processes   | %    | Loss processes  | %    |
|--|------|---|------|
| <b>Electrons</b>   |      |   |      |
| Electron impact ionization of Ar (2)   | 98.0 | Recombination with $H_3^+$ (18)                         | 94.2 |
| Fast $Ar^+$ ion impact ionization of Ar (20)                                 | 0.4  | Recombination with $H_2^+$ (17)                         | 2.7  |
| Fast $Ar^0$ atom impact ionization of Ar (57)                                | 1.3  | Recombination with $ArH^+$ (16)                         | 3.1  |
| Electron impact ionization of $H_2$ (11)                                     | 0.3  |   |      |
| <b><math>Ar^+</math> ions</b>  |      |   |      |
| Electron impact ionization of Ar (2)   | 97.9 | H-atom transfer between $Ar^+$ and $H_2$ (22)           | 87.1 |
| $Ar^+$ ion impact ionization of Ar (20)                                      | 0.4  | Charge transfer between $Ar^+$ and $H_2$ (23)           | 12.9 |
| $Ar^0$ atom impact ionization of Ar (57)                                     | 1.3  |   |      |
| Charge transfer between $H_2^+$ and Ar (38)                                  | 0.4  |   |      |
| <b><math>ArH^+</math> ions</b>   |      |   |      |
| H-atom transfer between $Ar^+$ and $H_2$ (22)                                | 88.7 | Proton transfer between $ArH^+$ and $H_2$ (28)          | 97.4 |
| Proton transfer between $H_2^+$ and Ar (37)                                  | 11.3 | Collision-induced dissociation of $ArH^+$ by Ar (25,26) | 2.4  |
|  |      | Recombination with electrons (16)                       | 0.2  |
| <b><math>H^+</math> ions</b>   |      |   |      |
| Collision-induced dissociation of $ArH^+$ by Ar (25)                         | 47.9 | Charge transfer between $H^+$ and Ar (31)               | 99.7 |
| Collision-induced dissociation of $H_3^+$ by Ar (45)                         | 21.0 | Charge transfer between $H^+$ and $H_2$ (35)            | 0.3  |
| Electron impact ionization of H atoms (14)                                   | 19.8 |   |      |
| Electron impact dissociative ionization of $H_2$ (12)                        | 11.3 |   |      |
| <b><math>H_2^+</math> ions</b>   |      |   |      |
| Charge transfer between $Ar^+$ and $H_2$ (23)                                | 88.4 | Proton transfer between $H_2^+$ and Ar (37)             | 82.1 |
| Electron impact ionization of $H_2$ (11)                                     | 11.5 | Charge transfer between $H_2^+$ and Ar (38)             | 16.8 |
|  |      | Proton transfer between $H_2^+$ and $H_2$ (39)          | 0.8  |
|  |      | Recombination with electrons (17)                       | 0.3  |
| <b><math>H_3^+</math> ions</b>   |      |   |      |
| Proton transfer between $ArH^+$ and $H_2$ (28)                               | 99.5 | Recombination with electrons (18)                       | 90.2 |
| Proton transfer between $H_2^+$ and $H_2$ (39)                               | 0.5  | Collision-induced dissociation of $H_3^+$ by Ar (45,46) | 9.0  |
|  |      | Charge transfer between $H_3^+$ and Ar (44)             | 0.7  |
| <b><math>H_2</math> molecules</b>  |      |   |      |
| Electron- $H_3^+$ recombination (18)   | 46.9 | Dissociation of $H_2$ by $Ar_m^*$ quenching (63)        | 62.5 |
| Charge transfer between $H_2^+$ and Ar (38)                                  | 45.3 | Electron impact dissociative excitation of $H_2$ (10)   | 24.2 |
| Collision-induced dissociation of $H_3^+$ by Ar (45)                         | 7.1  | Electron impact ionization of $H_2$ (11)                | 6.1  |
| Charge transfer between $H_3^+$ and Ar (44)                                  | 0.6  | Electron impact dissociative ionization of $H_2$ (12)   | 0.2  |
|  |      | H-atom transfer between $Ar^+$ and $H_2$ (22)           | 3.5  |
|  |      | Charge transfer between $Ar^+$ and $H_2$ (23)           | 3.5  |
| <b>H atoms</b>   |      |   |      |
| Dissociation of $H_2$ by $Ar_m^*$ quenching (63)                             | 63.0 | Recombination at the walls (66)                         | ~100 |
| Electron impact dissociative excitation of $H_2$ (10)                        | 24.4 |   |      |
| Electron impact dissociative ionization of $H_2$ (12)                        | 0.1  |   |      |
| Reflection of $H^+$ , $H_2^+$ , $H_3^+$ and $ArH^+$ at cathode (29,36,41,55) | 5.6  |   |      |
| Recombination of $H_2^+$ , $H_3^+$ and $ArH^+$ with electrons (16–18)        | 4.7  |   |      |
| H-atom transfer between $Ar^+$ and $H_2$ (22)                                | 1.8  |   |      |
| Collision-induced dissociation of $ArH^+$ by Ar (26)                         | 0.3  |   |      |
| Charge transfer between $H^+$ and Ar (31)                                    | 0.1  |   |      |
| <b><math>Ar_m^*</math> metastable atoms</b>                                  |      |   |      |
| Electron impact excitation of Ar (3)   | 25   | Diffusion and de-excitation at the walls (65)           | 46.7 |
| Fast $Ar^+$ ion impact excitation of Ar (21)                                 | 18   | Quenching by $H_2$ (dissociation of $H_2$ ) (63)        | 26.5 |
| Fast $Ar^0$ atom impact excitation of Ar (58)                                | 57   | Quenching by electrons (6)                              | 12.0 |
|  |      | Penning ionization of sputtered Cu atoms (60)           | 8.0  |
|  |      | Metastable–metastable collisions (59)                   | 3.5  |
|  |      | Electron impact excitation to higher levels (5)         | 2.3  |

conditions, with the new rate coefficient for  $ArH^+$ -electron recombination, and observed that recombination with  $H_3^+$  ions is indeed now dominant. Hence, the difference between our present and previous results<sup>20</sup> is not due to different operating conditions (VG9000 vs. Grimm-type), but simply due to the reduced value of the rate coefficient. However, this lowering of the rate coefficient did not affect the electron density to a large extent, so the other calculation results that we obtained in our previous papers<sup>20,21</sup> remain valid. When varying the  $H_2$  concentration, it appears that recombination with  $H_3^+$  ions is always the major loss mechanism for the electrons, but the relative contribution of recombination with  $H_2^+$  ions and  $ArH^+$

ions increases for lower  $H_2$  concentrations, to values of about 16% and 21.5%, respectively, at 0.1%  $H_2$  addition. At 10%  $H_2$  addition, on the other hand, it appears that the electrons get lost almost exclusively by recombination with  $H_3^+$  ions (calculated contribution of 99.3%). Indeed, their density increases more rapidly with  $H_2$  addition than the  $ArH^+$  density, as was illustrated in Fig. 2 above. Concerning the production of electrons, electron impact ionization of Ar atoms remains always the dominant production mechanism, but electron impact ionization of  $H_2$  atoms of course gains in importance for higher  $H_2$  concentrations, up to a calculated contribution of about 3.5% at 10%  $H_2$  addition.

Also the Ar<sup>+</sup> ions are mainly created by electron impact ionization, for all Ar–H<sub>2</sub> mixtures investigated. The relative contribution of charge transfer between H<sub>2</sub><sup>+</sup> ions and Ar atoms increases slightly with higher H<sub>2</sub> concentrations, up to a value of 2.6% calculated for 10% H<sub>2</sub> addition. The loss of Ar<sup>+</sup> ions is calculated to be mainly caused by H-atom transfer with H<sub>2</sub> molecules, although charge transfer also plays a non-negligible role. The relative contributions of both loss mechanisms were calculated to be more or less the same for all Ar–H<sub>2</sub> mixtures investigated.

This dominant loss mechanism for the Ar<sup>+</sup> ions, *i.e.*, H-atom transfer with H<sub>2</sub> molecules, represents also the most important production process for the ArH<sup>+</sup> ions, as is clear from Table 3. This is the case for all H<sub>2</sub> concentrations investigated. Concerning the loss of ArH<sup>+</sup> ions, proton transfer with H<sub>2</sub> molecules, to form H<sub>3</sub><sup>+</sup> ions, is the dominant loss mechanism, at all Ar–H<sub>2</sub> mixtures investigated, but especially at high H<sub>2</sub> concentrations. This explains why the H<sub>3</sub><sup>+</sup> ion density increases more upon H<sub>2</sub> addition than the ArH<sup>+</sup> ion density (see Fig. 2 above). At the lowest H<sub>2</sub> concentrations investigated, proton transfer is still the most important loss process, but collision-induced dissociation by Ar atoms becomes relatively more important, with a contribution of 17% calculated at 0.1% H<sub>2</sub> concentration.

The latter process is the most significant production mechanism for the H<sup>+</sup> ions, especially at low H<sub>2</sub> concentrations (for instance, the relative contribution was calculated to be 48% at 1% H<sub>2</sub> addition (see Table 3), and 61% at 0.1% H<sub>2</sub> concentration). At higher H<sub>2</sub> concentrations, collision-induced dissociation of H<sub>3</sub><sup>+</sup> ions by Ar atoms becomes gradually more important, with a calculated relative contribution of 61% at 10% H<sub>2</sub> addition. Also electron impact ionization of H atoms and dissociative ionization of H<sub>2</sub> molecules play a non-negligible role in the production of H<sup>+</sup> ions. Charge transfer with Ar atoms is the dominant loss process for the H<sup>+</sup> ions, at all conditions investigated, although charge transfer with H<sub>2</sub> molecules becomes gradually more important, with a relative contribution of 4.4% calculated for 10% H<sub>2</sub> addition.

The H<sub>2</sub><sup>+</sup> ions are mainly produced by charge transfer between Ar<sup>+</sup> ions and H<sub>2</sub> molecules, and they are destructed by proton transfer (or to a smaller extent by charge transfer) with Ar atoms. These relative contributions are more or less the same for all Ar–H<sub>2</sub> mixtures investigated, but at higher H<sub>2</sub> concentrations, electron impact ionization of H<sub>2</sub> molecules gains importance as a production process (with a relative contribution calculated to be 23% at 10% H<sub>2</sub> addition), whereas proton-transfer between H<sub>2</sub><sup>+</sup> ions and H<sub>2</sub> molecules becomes non-negligible as a loss mechanism (with a relative contribution of 9% calculated for 10% H<sub>2</sub> addition).

The H<sub>3</sub><sup>+</sup> ions are almost exclusively produced by proton transfer between ArH<sup>+</sup> ions and H<sub>2</sub> molecules, as mentioned above, and they are destructed mainly by recombination with electrons, although collision-induced dissociation by Ar atoms also contributes for about 10%. This is true for all Ar–H<sub>2</sub> mixtures investigated.

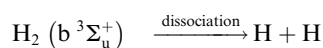
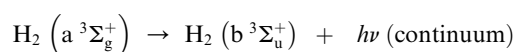
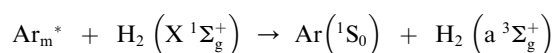
As far as the H<sub>2</sub> molecules are concerned, their production by chemical reactions in the plasma is of course not so significant, because they are present as a background gas. Nevertheless, small fractions of H<sub>2</sub> molecules are produced, mainly by electron–H<sub>3</sub><sup>+</sup> recombination and charge transfer between H<sub>2</sub><sup>+</sup>

ions and Ar atoms. The first process is especially important at high H<sub>2</sub> concentrations (with a relative contribution calculated to be 63% at 10% H<sub>2</sub> addition), whereas the latter process is dominant at low H<sub>2</sub> concentrations (*e.g.*, 92% at 0.1% H<sub>2</sub> addition). The loss of H<sub>2</sub> molecules is mainly attributed to dissociation by quenching of Ar<sub>m</sub><sup>\*</sup> metastable atoms, but electron impact dissociative excitation and ionization gain importance upon increasing H<sub>2</sub> addition. Indeed, their relative contribution is about 17 and 5%, respectively at 0.1% H<sub>2</sub> addition, *vs.* 71% for Ar<sub>m</sub><sup>\*</sup> quenching; at 1% H<sub>2</sub> concentration, the relative roles of these three processes are about 24%, 6% and 63%, as is clear from Table 3; and at 10% H<sub>2</sub> addition, electron impact dissociative excitation and ionization contribute at 37 and 12%, respectively, whereas the role of Ar<sub>m</sub><sup>\*</sup> quenching has dropped to about 36%.

The H atoms are mainly generated by this process of Ar<sub>m</sub><sup>\*</sup> quenching, resulting in H<sub>2</sub> dissociation, especially at low H<sub>2</sub> concentrations (*i.e.*, relative contribution calculated to be 74% at 0.1% H<sub>2</sub> concentration, decreasing to 63% at 1% H<sub>2</sub> fraction, and to 32% at 10% H<sub>2</sub> addition). On the other hand, the relative role of electron impact dissociative excitation increases as production mechanism, from 17% at 0.1% H<sub>2</sub> concentration, to 24% at 1% H<sub>2</sub> fraction, and 34% at 10% H<sub>2</sub> addition. Also electron–H<sub>3</sub><sup>+</sup> ion recombination plays a non-negligible role as production mechanism, with a relative contribution of 21% at 10% H<sub>2</sub> addition. Besides, reflection (and dissociation/neutralization) of H<sup>+</sup>, H<sub>2</sub><sup>+</sup>, H<sub>3</sub><sup>+</sup> and ArH<sup>+</sup> ions bombarding at the walls also contribute to some production of the H atoms. Likewise, the H atoms almost exclusively disappear from the plasma by recombination at the walls, resulting in formation of H<sub>2</sub> molecules.

Finally, the Ar<sub>m</sub><sup>\*</sup> atoms are populated by electron, fast Ar<sup>+</sup> ion and especially fast Ar atom impact excitation of Ar ground state atoms. The latter explains the pronounced peak in their density near the cathode (see Fig. 3 above), as fast Ar<sup>+</sup> ion and Ar<sup>0</sup> atom impact excitation are only important near the cathode. Loss of the Ar<sub>m</sub><sup>\*</sup> metastable atoms is mainly attributed to de-excitation at the walls, but quenching by dissociation of H<sub>2</sub> molecules plays also an important role, especially at higher H<sub>2</sub> concentrations. Indeed, the relative role of this process increases from 4% at 0.1% H<sub>2</sub> fraction, to 26.5% at 1% H<sub>2</sub> concentration, to almost 70% at 10% H<sub>2</sub> addition. This explains why the Ar<sub>m</sub><sup>\*</sup> metastable density, as well as the relative importance of Penning ionization for the sputtered atoms, drops at high H<sub>2</sub> concentrations.

Finally, it is worth mentioning that our calculations predict that the dissociation of H<sub>2</sub> molecules into H atoms occurs predominantly by quenching of Ar<sub>m</sub><sup>\*</sup> metastable atoms, rather than by electron impact dissociative excitation. This is in agreement with experimental observations of a strong continuum emission in the spectral range 220–440 nm, in Ar/H<sub>2</sub> glow discharges.<sup>14–16</sup> This continuum is considered to be the result of the sequence:<sup>14–16,30</sup>



An alternative reaction path would be the excitation into the triplet state by electron impact, followed also by dissociation (*i.e.*, reaction no. 10 of Table 2). However, in Ne/H<sub>2</sub> mixtures, where excitation of the H<sub>2</sub> molecules by Ne metastables is not possible, no significant continuum was observed under similar experimental conditions.<sup>16</sup> This suggests, indeed, that electron impact dissociative excitation is less important than dissociative excitation by Ar metastables, in agreement with our model predictions.

#### 4. Conclusion

A comprehensive model developed previously for Ar–H<sub>2</sub> gas mixtures has been applied to a Grimm-type glow discharge, and the effect of H<sub>2</sub> additions varying between 0.1 and 10% has been investigated on the densities of the various plasma species, their production and loss mechanisms, the electrical current, and the sputtering process. It is found that beside the Ar<sup>+</sup> ions, also the ArH<sup>+</sup> and H<sub>3</sub><sup>+</sup> ions are important positive ions in the discharge, especially at higher H<sub>2</sub> concentrations. The H<sup>+</sup> and H<sub>2</sub><sup>+</sup> ions are of minor importance. The dissociation degree of the H<sub>2</sub> molecules was calculated to be around 1–2%, which is significantly higher than at typical VG9000 GDMS conditions. This is attributed to the higher gas pressure, resulting in more dissociation collisions of the H<sub>2</sub> molecules. The density of sputtered Cu atoms is not so much affected by the H<sub>2</sub> addition to the discharge, because on one hand, the Ar<sup>+</sup> ion flux decreases upon H<sub>2</sub> addition, but on the other hand, the fluxes of hydrogen-related ions increase. Hence, the relative contribution of Ar<sup>+</sup> ions to the sputtering process decreases, whereas the ArH<sup>+</sup> ions gain importance, so that the rate of sputtering remains very similar. For the same reason, the calculated electrical current appears not to be strongly affected by the Ar–H<sub>2</sub> gas mixture. The Ar<sub>m</sub>\* metastable atoms, on the other hand, are characterized by a significant drop in their density for high enough H<sub>2</sub> concentrations, due to Ar<sub>m</sub>\* quenching by dissociation of H<sub>2</sub> molecules. This process might be responsible for the strong continuum emission in the spectral range 220–440 nm, in Ar/H<sub>2</sub> glow discharges.<sup>14–16</sup> Moreover, because of the decreasing Ar<sub>m</sub>\* density, the role of Penning ionization of sputtered Cu atoms is also expected to become lower for high enough H<sub>2</sub> additions. Electron impact ionization, on the other hand, becomes relatively more important, and this is, at least qualitatively, in accordance with literature observations on the comparison between measured RSFs in GDMS with predictions from simple equilibrium models.<sup>6,7</sup>

We have tried to compare our calculation results as much as possible with experimental data available in the literature, and we were able to find reasonable explanations for most experimental observations and trends. Exact detailed comparison is often difficult. For instance, in the present calculations no gas heating and gas flow were taken into account. We don't think that this will have a large impact on the plasma chemistry; however, it means that our calculation results might not be applicable to conditions where the gas flow is essential.<sup>4,5</sup> Indeed, such fast-flow glow discharge cells can generate a secondary plasma, as was recently demonstrated by Voronov and Hoffmann,<sup>31</sup> and this might further complicate the situation.

Finally, note that our model is not yet able to predict trends in optical emission line intensities as a function of H<sub>2</sub> addition in GD-OES. For this purpose, information is needed on the excited level populations of H atoms, H<sub>2</sub> molecules and sputtered atoms and ions. In the near future, a collisional-radiative model will be developed, describing the behavior of excited levels of H atoms and H<sub>2</sub> molecules, in connection with the excited levels of Ar and sputtered atoms, with the purpose to explain why different optical emission lines behave differently upon H<sub>2</sub> addition.

#### Acknowledgements

The author would like to thank B. Mitchell and N. Konjevic for pointing out a newly available rate coefficient of ArH<sup>+</sup>–electron recombination, and E. Steers for his advise on applying the model to the Grimm-type conditions. This research is financially supported by the European Marie Curie Research Training Network GLADNET (Contract N° MRTN-CT-2006 035459). The calculations were performed on the CALCUA supercomputer facilities of the University of Antwerp.

#### References

- 1 M. Kuraica and N. Konjevic, *Phys. Rev. A*, 1992, **46**, 4429.
- 2 M. Kuraica, N. Konjevic, M. Platisa and D. Pantelic, *Spectrochim. Acta, Part B*, 1992, **47**, 1173.
- 3 I. R. Videnovic, N. Konjevic and M. Kuraica, *Spectrochim. Acta, Part B*, 1996, **51**, 1707.
- 4 R. S. Mason, P. D. Miller and I. P. Mortimer, *Phys. Rev. E*, 1997, **55**, 7462.
- 5 K. Newman, R. S. Mason, D. R. Williams and I. P. Mortimer, *J. Anal. At. Spectrom.*, 2004, **19**, 1192.
- 6 R. W. Smithwick III, D. W. Lynch and J. C. Franklin, *J. Am. Soc. Mass Spectrom.*, 1993, **4**, 278.
- 7 M. Saito, *Anal. Chim. Acta*, 1997, **355**, 129.
- 8 A. Menendez, J. Pisonero, R. Pereiro, N. Bordel and A. Sanz-Medel, *J. Anal. At. Spectrom.*, 2003, **18**, 557.
- 9 A. Menendez, R. Pereiro, N. Bordel and A. Sanz-Medel, *Spectrochim. Acta, Part B*, 2005, **60**, 824.
- 10 A. Menendez, R. Pereiro, N. Bordel and A. Sanz-Medel, *J. Anal. At. Spectrom.*, 2006, **21**, 531.
- 11 A. Martin, A. Menéndez, R. Pereiro, N. Bordel and A. Sanz-Medel, *Anal. Bioanal. Chem.*, 2007, **388**, 1573.
- 12 A. Fernandez, N. Bordel, C. Perez, R. Pereiro and A. Sanz-Medel, *J. Anal. At. Spectrom.*, 2002, **17**, 1549.
- 13 A. Martin, R. Pereiro, N. Bordel and A. Sanz-Medel, *Spectrochim. Acta, Part B*, 2008, **63**, 692.
- 14 V.-D. Hodoroba, V. Hoffmann, E. B. M. Steers and K. Wetzig, *J. Anal. At. Spectrom.*, 2000, **15**, 951.
- 15 V.-D. Hodoroba, V. Hoffmann, E. B. M. Steers and K. Wetzig, *J. Anal. At. Spectrom.*, 2000, **15**, 1075.
- 16 V.-D. Hodoroba, E. B. M. Steers, V. Hoffmann and K. Wetzig, *J. Anal. At. Spectrom.*, 2001, **16**, 43.
- 17 Z. Weiss, E. B. M. Steers and P. Smid, *J. Anal. At. Spectrom.*, 2005, **20**, 839.
- 18 V. D. Hodoroba, E. B. M. Steers, V. Hoffmann, W. E. S. Unger, W. Paatsch and K. Wetzig, *J. Anal. At. Spectrom.*, 2003, **18**, 521.
- 19 E. B. M. Steers, P. Smid and Z. Weiss, *Spectrochim. Acta, Part B*, 2006, **61**, 414.
- 20 A. Bogaerts and R. Gijbels, *Spectrochim. Acta, Part B*, 2002, **57**, 1071.
- 21 A. Bogaerts, *J. Anal. At. Spectrom.*, 2002, **17**, 768.
- 22 A. Bogaerts and R. Gijbels, *Phys. Rev. E*, 2002, **65**, 056402.
- 23 N. Matsunami, Y. Yamamura, Y. Itikawa, N. Itoh, Y. Kazumata, S. Miyagawa, K. Morita, R. Shimizu and H. Tawara, *At. Data Nucl. Data Tables*, 1984, **31**, 1–80.
- 24 R. F. G. Meulenbroeks, A. J. van Beek, A. J. G. van Helvoort, M. C. M. van de Sanden and D. C. Schram, *Phys. Rev. E*, 1994, **49**, 4397.

- 
- 25 J. B. A. Mitchell, O. Novotny, J. L. DeGarrec, A. Florescu-Mitchell, C. Rebrion-Rowe, A. V. Stolyarov, M. S. Child, A. Svendsen, M. A. El Ghazaly and L. H. Andersen, *J. Phys. B*, 2005, **38**, L175.
- 26 B. J. Wood and H. Wise, *J. Chem. Phys.*, 1958, **29**, 1416.
- 27 A. C. Dexter, T. Farrell and M. I. Lees, *J. Phys. D*, 1989, **22**, 413.
- 28 T. Simko, V. Martisovits, J. Bretagne and G. Gousset, *Phys. Rev. E*, 1997, **56**, 5908.
- 29 P. H. Ratliff and W. W. Harrison, *Spectrochim. Acta, Part B*, 1994, **49**, 1747.
- 30 C. R. Lishawa, J. W. Feldstein, T. N. Stewart and E. E. Muschlitz, Jr, *J. Chem. Phys.*, 1985, **83**, 133.
- 31 M. Voronov and V. Hoffmann, *J. Anal. At. Spectrom.*, 2007, **22**, 1184.